

## Three-dimensional diastolic blood flow in the left ventricle

Khalafvand, Seyed Saeid; Ng, Eddie Yin Kwee; Zhong, Liang; Hung, Tin Kan

**DOI**

[10.1016/j.jbiomech.2016.11.032](https://doi.org/10.1016/j.jbiomech.2016.11.032)

**Publication date**

2017

**Document Version**

Final published version

**Published in**

Journal of Biomechanics

**Citation (APA)**

Khalafvand, S. S., Ng, E. Y. K., Zhong, L., & Hung, T. K. (2017). Three-dimensional diastolic blood flow in the left ventricle. *Journal of Biomechanics*, 50, 71-76. <https://doi.org/10.1016/j.jbiomech.2016.11.032>

**Important note**

To cite this publication, please use the final published version (if applicable). Please check the document version above.

**Copyright**

Other than for strictly personal use, it is not permitted to download, forward or distribute the text or part of it, without the consent of the author(s) and/or copyright holder(s), unless the work is under an open content license such as Creative Commons.

**Takedown policy**

Please contact us and provide details if you believe this document breaches copyrights. We will remove access to the work immediately and investigate your claim.



## Three-dimensional diastolic blood flow in the left ventricle



Seyed Saeid Khalafvand<sup>a,b</sup>, Eddie Yin-Kwee Ng<sup>a</sup>, Liang Zhong<sup>c,d</sup>, Tin-Kan Hung<sup>e,\*</sup>

<sup>a</sup> School of Mechanical and Aerospace Engineering, College of Engineering, Nanyang Technological University, 50 Nanyang Avenue, Singapore 639798, Singapore

<sup>b</sup> Faculty of Applied Science, Delft University of Technology, 2629 HZ Delft, The Netherlands

<sup>c</sup> Duke-NUS Medical School Singapore 8 College Road Singapore 169857 Singapore

<sup>d</sup> National Heart Research Institute Singapore, National Heart Centre Singapore 5 Hospital Drive 169609 Singapore

<sup>e</sup> Department of Bioengineering, University of Pittsburgh Pittsburgh PA 15261 USA

### ARTICLE INFO

#### Article history:

Accepted 2 November 2016

#### Keywords:

Blood flow  
Left ventricle  
Navier–Stokes equation  
Vortices  
Work energy equation

### ABSTRACT

Three-dimensional blood flow in a human left ventricle is studied via a computational analysis with magnetic resonance imaging of the cardiac motion. Formation, growth and decay of vortices during the myocardial dilation are analyzed with flow patterns on various diametric planes. They are dominated by momentum transfer during flow acceleration and deceleration through the mitral orifice. The posterior and anterior vortices form an asymmetric annular vortex at the mitral orifice, providing a smooth transition for the rapid inflow to the ventricle. The development of core vortex accommodates momentum for deceleration and for acceleration at end diastolic atrial contraction. The rate of energy dissipation and that of work done by viscous stresses are small; they are approximately balanced with each other. The kinetic energy flux and the rate of work done by pressure delivered to blood from ventricular dilation is well balanced by the total energy influx at the mitral orifice and the rate change of kinetic energy in the ventricle.

Published by Elsevier Ltd.

### 1. Introduction

Study of blood flow in the left ventricle (LV) is to identify cardiac function and dysfunction. Using magnetic resonance velocity mapping, Kim et al. (1995) reported a large counterclockwise vortex in the ventricle during diastole. Kilner et al. (2000) indicated that flow patterns in the normal LV do not have excessive energy loss for blood ejection from the left ventricle. Asymmetric vortices were reported by many investigators (Baccani et al., 2002, 2003; Ebbers et al., 2002; Vierendeels et al., 2000; Saber et al., 2003, 2001). Pedrizzetti and Domenichini (2005) and Domenichini et al. (2005) presented flow patterns in a prolate spheroid CFD model, discussing the normal heart motion being optimal in term of minimal energy dissipation. Long et al. (2003, 2008) reported a main counterclockwise vortex during the inflow and the influence of boundary motion to flow patterns. Schenkel et al. (2009) studied asymmetry vortices with time-dependent mitral and aortic orifices without modeling valve leaflet movements. Other CFD modeling included immerse boundary (IB) methods (McQueen and Peskin, 1989, 1997; McQueen and Peskin, 2000) and fluid-structure interaction (FSI) methods (Cheng et al., 2005; Krittian

et al., 2010; Watanabe et al., 2004). The majorities of the LV numerical simulations were focused on normal subjects to understand the LV fluid dynamics, while some studies considered the patient-specific LVs in heart failure (Khalafvand et al., 2014). From magnetic resonance phase-contrast velocity mapping, Bolger et al. (2007) showed the kinetic energy of inflow for normal and dilated left ventricles. Hung et al. (2008) employed velocity vectors of echocardiogram to show kinetic energy flux for normal and dys-synchrony ventricular contractions. Faludi et al. (2010) discussed low resolutions of echocardiographic 3D imaging technology and vortex formations in healthy left ventricles. Using an echocardiographic method, Uejima et al. (2010) showed vortex flow patterns for inflow to the ventricle. Eriksson et al. (2011) studied pathlines traced in 25 ms during an onset mitral flow. From 2D phase contrast MRI Charonko et al. (2013) calculated temporal variations of pressure drop and kinetic energy of the mitral flow for 12 subjects.

The present study is focused on kinematic, dynamic and energy characteristics of diastolic flow in a normal left ventricle motion. The 3D flow patterns are presented by spiral streamlines and analyzed by the Lagrange stream function (2D streamlines) on various longitudinal sections. This approach shows the development of anterior and posterior vortices, resulting in an asymmetric ring vortex during the rapid filling phase of blood to the ventricle. A counterclockwise core vortex is formed during diastolic flow

\* Corresponding author.

E-mail address: [tkhung@pitt.edu](mailto:tkhung@pitt.edu) (T.-K. Hung).

deceleration, followed by momentum transfer from the main flow to vortices during end diastolic acceleration and deceleration. The inflow characteristics are further studied using the work-energy equation. The kinetic energy flux and the rate of work done by pressure during cardiac dilation are calculated for energy transfer in the ventricle. The rate of work done by shear stresses and energy dissipation are obtained to be relatively very small.

## 2. Methods

### 2.1. MRI geometry reconstruction and grid generation

MRI scanning was performed on a healthy adult with a 1.5T Siemens scanner using steady state free precession cine gradient echo sequences (Avanto, Siemens Medical Solutions, Erlangen). The ventricular 2-chamber, 4-chamber, and short-axis planes were acquired with 12–14 equidistant slices for the left ventricle and atrium. The field of view was typically 320 mm with in-plane spatial resolution less than 1.5 mm. Each slice was acquired in a single breath hold, with 25 temporal phases per cardiac cycle. The reconstruction of LV geometry for CFD simulation was made by using a semi-automatic method. Fig. 1a shows the ventricle at end-diastole and end-systole. For each time step, unstructured grids consisting of tetrahedral cells were generated using a semi-automatic method. The grid topology for the computational domain is shown in Fig. 1b. To obtain a refined resolution, intermediate time steps and geometries were generated by cubic spine functions. To have the Courant number less than unity, 75 time steps were generated for each interval of the 25 geometries, resulting in 1800 time steps ( $=24 \times 75$ ) for one cardiac cycle of computation. The velocities on the LV wall were calculated from differences between the current and former grids. To find an optimum number of elements (cells) for modelling of the LV chamber, the grid convergence index (GCI) was used for assessing grid invariant solution (Roache, 1998). A grid dependency study was

made for five different cases with number of finite volumes increased from 50,000 to 75,000; 112,500; 168,750 and 253,125. Test results indicated that flow features obtained from 112,500 and 168,750 finite volumes were practically the same. The latter was chosen for this study.

### 2.2. The Navier–Stokes equations

The filling and ejection of blood flow in the left ventricle are calculated by using a finite volume method for the arbitrary Lagrangian–Eulerian (ALE) formulation of the Navier–Stokes equations. The integral form of the continuity equation for a volume ( $dV$ ) with surface ( $S$ ) is expressed as

$$\frac{\partial}{\partial t} \int_V \rho dV + \int_S \rho (\vec{v} - \vec{v}_b) \cdot \vec{n} dS = 0 \quad (1)$$

where  $\vec{v}$  is the velocity vector,  $\vec{v}_b$  the velocity on the boundary,  $\vec{n}$  the normal vector and  $\rho$  the blood density. The momentum equation is

$$\int_V \frac{\partial}{\partial t} (\rho \vec{v}) dV + \int_S \rho \vec{v} (\vec{v} - \vec{v}_b) \cdot \vec{n} dS = - \int_S p \mathbf{I} \cdot \vec{n} dS + \int_S \boldsymbol{\tau} \cdot \vec{n} dS \quad (2)$$

where  $p$  is the pressure,  $\mathbf{I}$  the unit tensor, and  $\boldsymbol{\tau}$  the viscous stress tensor. Blood flowing in large arteries can be treated as homogeneous Newtonian fluid with density of  $1050 \text{ kg m}^{-3}$  and the dynamic viscosity of  $0.00316 \text{ Pa s}$ . Computational results are obtained from the MRI data of an adult with end systolic volume of  $48.8 \text{ ml}$  and end diastolic volume of  $162.5 \text{ ml}$ , resulting in a normal stroke volume of  $113.7 \text{ ml}$  and a normal ejection fraction of 70%. The cardiac period ( $T$ ) is  $0.88 \text{ s}$  with  $0.55 \text{ s}$  of diastole and  $0.33 \text{ s}$  of systole (see Fig. 2). The normalized temporal ventricle volume based on a set of 25 LV geometries during the cardiac period is shown in Fig. 2a. The periodic flow patterns are computed from an initial hydrostatic condition with the motion of the left ventricle and atrium, velocity  $V_D(t)$  at the atrial inlet for diastole, and no flow at the aortic outlet. The inclusion of the left atrium is to facilitate modeling inflow to the mitral orifice. During systole velocity  $V_O(t)$  is prescribed at the outlet with no flow at the atrial inlet. Because of the non-circular inlet and outlet, the instantaneous hydraulic radius is used to define the

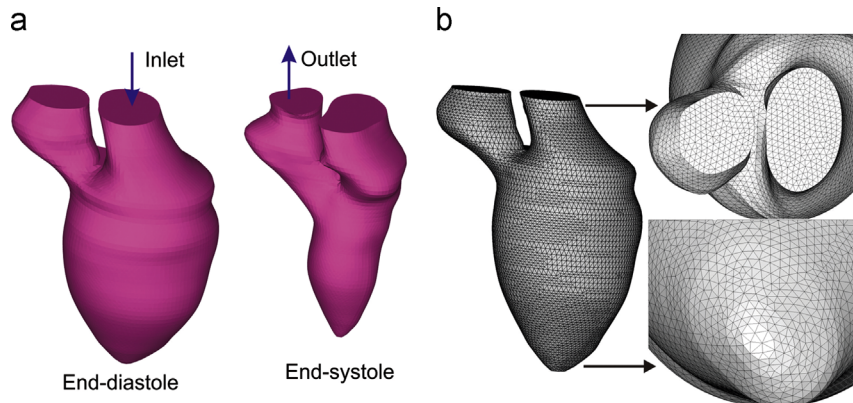


Fig. 1. (a) Reconstruction of left ventricle geometries, left atrium and ascending aorta at end-diastole and end-systole. (b) Grid topology of proximal left atrium and ascending aorta.

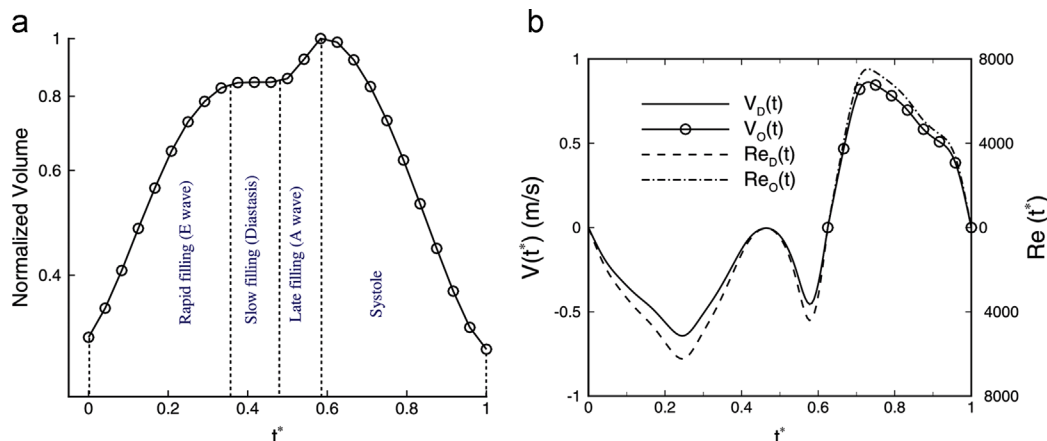
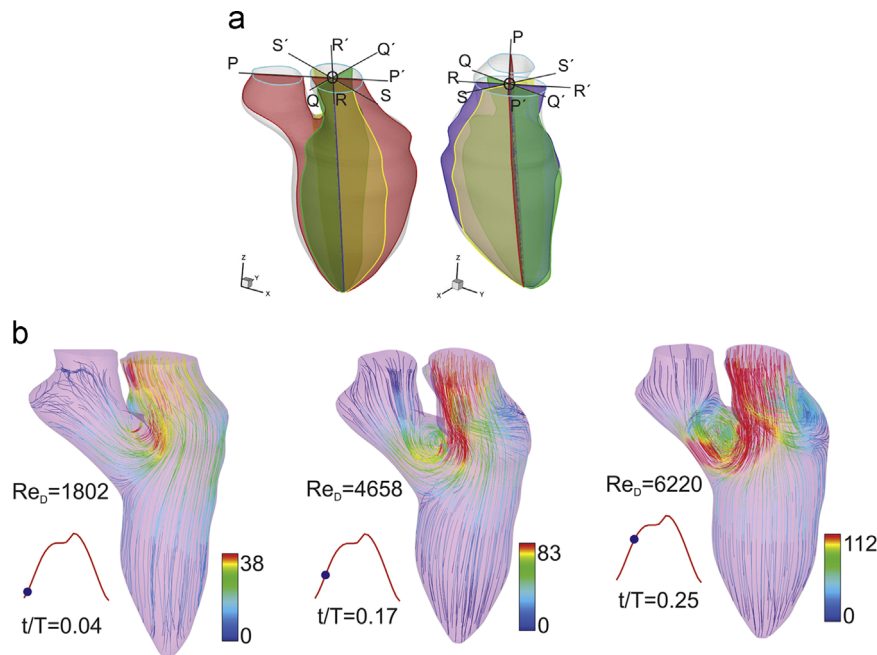


Fig. 2. (a) Temporal variation of the left ventricle volume;  $t^* = t/T = 0$  for the onset diastole and  $t^* = 1$  for end systole. (b) Temporary variation of velocity  $V_D(t)$  and  $Re_D(t)$  at inlet for diastolic flow;  $V_O(t)$  and  $Re_O(t)$  at outlet of systolic flow.



**Fig. 3.** (a) Longitudinal sections: P–P', Q–Q', R–R' and S–S'. (b) Spiral streamlines of the accelerated diastolic flow with the Reynolds number,  $Re_D$ , rising rapidly from zero to 1802, 4658 and 6220. Streamlines colored by velocity magnitude (cm/s).

transient Reynolds number  $Re_D(t)$  for diastolic flow. The corresponding flow rate can be evaluated by  $Re_D^2(t)\mu^2\pi/4\rho^2V_D(t)$ . The difference between  $Re_D(t)$  and  $V_D(t)$  is due to the time varied mitral orifice. The Navier–Stokes equations are solved using the finite volume CFD solver ANSYS Fluent. The dynamic mesh in ANSYS Fluent is based on the ALE formulation. The motion of ventricle is implemented with the user defined functions (UDFs). The grid quality is monitored by the face skew angle below  $40^\circ$ , and the re-meshing software in ANSYS Fluent is applied when the grid quality is to be improved. The twist motion of the ventricle was not obtained in MRI nor considered in the CFD computation. The PISO (pressure implicit with splitting of operators) algorithm (Issa, 1986) is employed along with a second order upwind scheme. In the present study, the pulsating flow was computed using unstructured grids without modelling the mitral valve motion. This simplification made the CFD much easier; it was supported by the results of two 2D models, one with mitral valve motion and the other without. The flow resistance due to the mitral leaflets was small.

### 3. Results and discussion

#### 3.1. Diastolic flow characteristics

The periodic solutions for diastolic and systolic flows were obtained after 4 cycles of computation. Since the spiral flow patterns with vortices are very complicated, they are dissected and analyzed from 2D flow patterns obtained from the Lagrange stream function on several longitudinal sections: P–P', Q–Q', R–R' and S–S' planes shown in Fig. 3a. Fig. 3b shows streamlines of the accelerated diastolic flow with the Reynolds number,  $Re_D$ , rising rapidly from zero to 1802, 4658 and 6220 in 0.22 s ( $t/T=0.25$ ). The curvature effect of the accelerated flow results in high velocities at the aortic-mitral junction with a clockwise 3D vortex along with a counter clockwise vortex developed on the anterior side. The flow is then decelerated by ventricular dilation with  $Re_D$  reduced to 3856 at  $t=0.29$  s. The 3D spiral flow shown in the northwest corner of Fig. 4a is accompanied by 2D flow patterns on various sections including the PQ–P'Q' section (a diagonal midsection between P–P' and Q–Q'). Notice that the counter clockwise vortex exceeds the arch of SP'Q'R' and is connected to the clockwise vortex, forming a ring vortex. This vortex would be larger if the mitral leaflet movements were included in the modeling. During this rapid filling phase, the flow patterns in the lower part of LV are dominated by the dilating myocardium. At this time about 70%

of stroke volume is filled in the ventricle and most of the flow region remains vortex free. Similar to laminar flow separation reported by Macagno and Hung (1967), the flow separation shown in Fig. 4a and b provides a smooth transition for inflow to the ventricle. As the Reynolds number decreases to 46 at  $t^*=t/T=0.46$  (refer to Fig. 4b) the reduced main flow results in momentum transfer for a rapid growth of the counter clockwise vortex, occupying most part of the ventricle. The vortex structure can be seen from flow patterns on various sections. On the P–P' section, the counterclockwise vortex is elongated and bottlenecked with dual centers. The vortex extends circumferentially to sections S–S', RS–R'S' (the midsection between R–R' and S–S') and Q–Q'. The counter clockwise core vortex remains connected to the clockwise one (below RQPS') as a ring vortex. The rapid growth of vortices is due to momentum transfer from the main flow during deceleration (Hung and Tsai, 1997). Since velocities on the boundary move with LV dilation, viscous effect is expected to be small and is quantified by energy dissipation in Section 3.2. The remaining diastolic flow is associated with the left atrium contraction. Fig. 5a shows flow pattern when  $Re_D$  rises from 46 to 2394 in 0.074 s. The inflow momentums move towards the inter-ventricular septum region, breaking up the ring vortex and forming a large counterclockwise vortex in the ventricle. The wall dilation dominates the flow pattern on section Q–Q'. At  $t/T=0.54$  the Reynolds number reaches 2394 then to 4358 (see Fig. 5b). The crescent vortex can be seen by the vortex center on each of P–P', S–S' and R–R' sections, indicating a strong circulatory motion in the core. In short, the momentum of the end diastolic contraction (due to the A-wave) merges and strengthens the vortices and main flow. The diastolic flow reduces rapidly thereafter and  $Re_D$  is equal to zero at  $t=0.54$  s ( $t/T=0.63$ ; see Fig. 6). As indicated by the flow patterns on P–P', S'–S, RS–R'S' and R–R' sections, the counterclockwise vortex occupies almost the entire region with vortex splitting to two pockets. They are associated with momentum transfer in the curvilinear flow deceleration. Although the inflow vanishes, slight wall movements remain visible in these 2D flow patterns. Also shown in Fig. 6 are velocity vectors on cross sections H1 and H2 (refer to Fig. 3a), indicating 3D spiral flow in the ventricle.

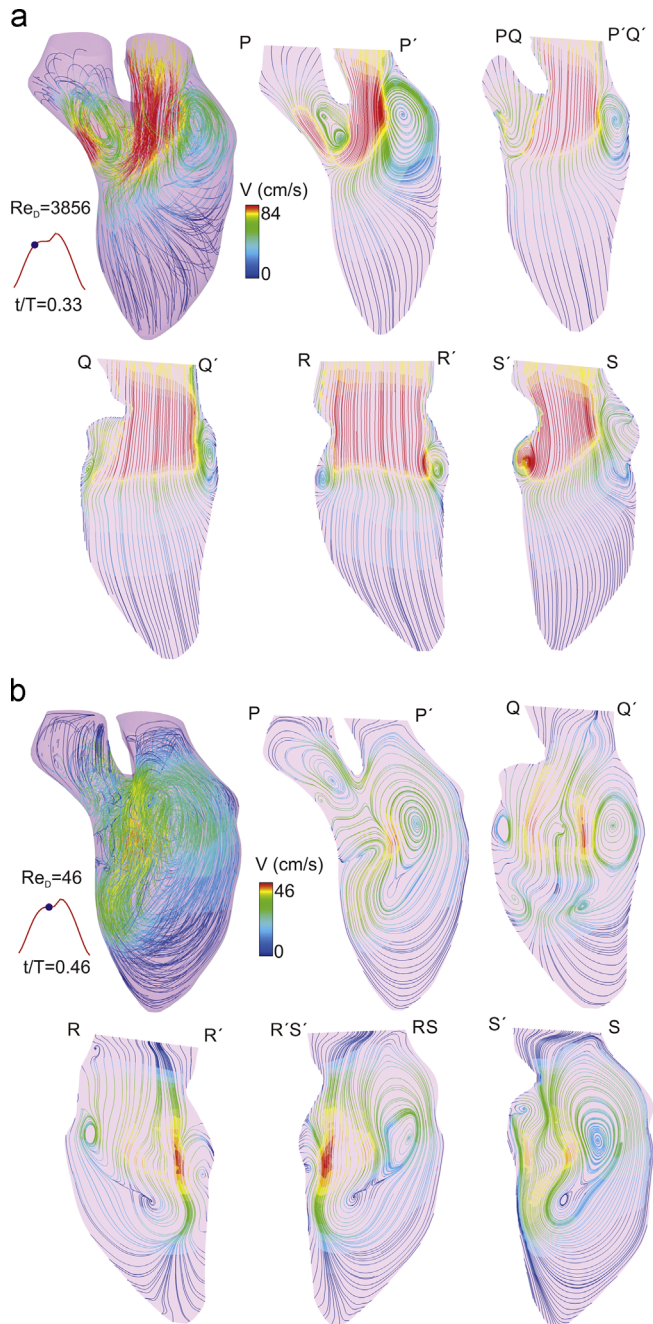


**Fig. 4.** Flow patterns during (a) diastolic deceleration;  $t/T=0.33$  (b) slow filling phase of diastole;  $t/T=0.46$ .

**Fig. 7a** correlates the time variation of the Reynolds number  $Re_D(t)$  with the results of pressure difference  $\Delta P_D(t)$  between the apex and the center of the mitral annulus. Both of them are plotted downward for inflow to the ventricle. Because of rapid flow acceleration and deceleration, the peak  $\Delta P_D(t)$  precedes the peak inflow and is in phase with flow acceleration. They are produced by ventricular dilatation due to elastic energy stored in myocardium during contraction. **Fig. 7b** compares pressure drops obtained from two 2D-models, one with and the other without the mitral valve (Hung et al., 2015; Khalafvand et al., 2015). The difference between them indicates a small additional pressure drop for the mitral valve motion. Since the inflow velocity  $V_D(t)$  is the same as that for the 3D model, the pressure drops for the 2D and 3D models are comparable.

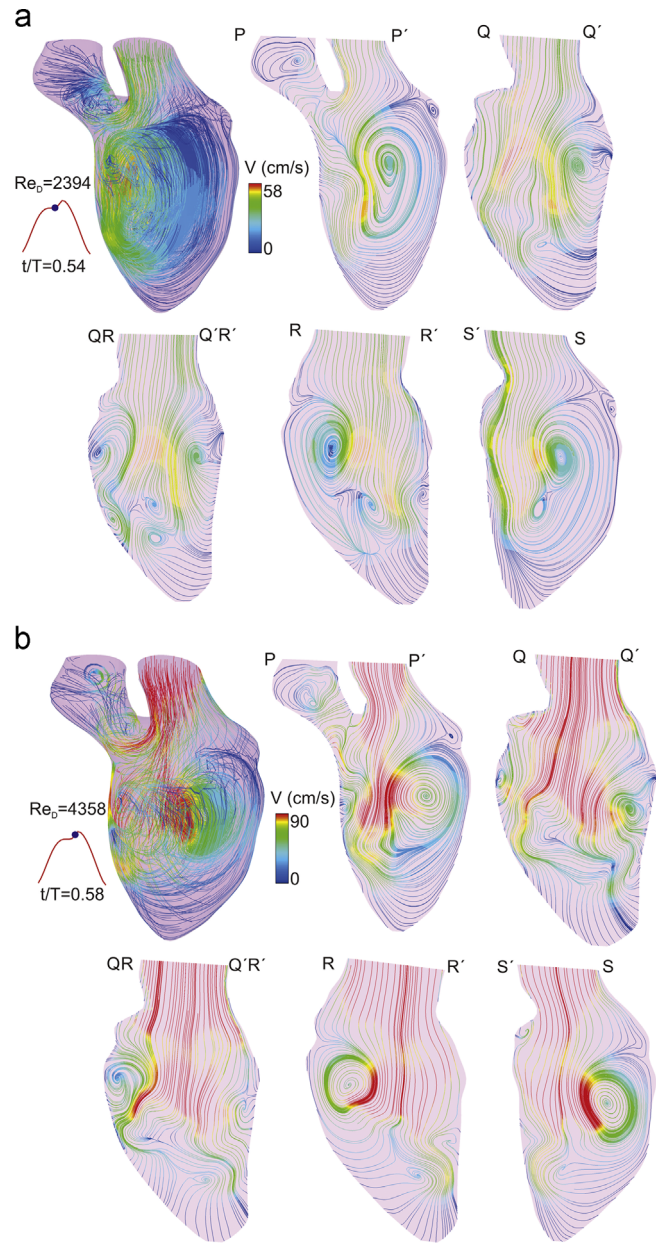


**Fig. 5.** Flow patterns during (a) late filling phase (re-filling) of diastole;  $t/T=0.54$  (b) late filling phase of diastole;  $t/T=0.58$ .

### 3.2. Energy transfer characteristics

The fluid mechanics of cardiac pumping can be learned further from an analysis using the integral form of the work-energy equation (Brown and Hung, 1977; Macagno and Hung, 1967):

$$\begin{aligned} & \iint_W \left( \frac{\rho V^2}{2} + p \right) V_N dS + \iiint \left( \frac{\rho}{2} \frac{\partial V^2}{\partial t} \right) dx dy dz - \iint_m \left( \frac{\rho V_m^2}{2} + p_m \right) V_m dS \\ & - \iint_W \vec{V} \cdot \vec{\tau} dS + \iiint \mu \left( 2 \left( \frac{\partial u}{\partial x} \right)^2 + 2 \left( \frac{\partial v}{\partial y} \right)^2 + 2 \left( \frac{\partial w}{\partial z} \right)^2 + \left( \frac{\partial u}{\partial y} + \frac{\partial v}{\partial x} \right)^2 \right. \\ & \left. + \left( \frac{\partial u}{\partial z} + \frac{\partial w}{\partial x} \right)^2 + \left( \frac{\partial w}{\partial y} + \frac{\partial v}{\partial z} \right)^2 \right) dx dy dz = 0 \end{aligned} \quad (3)$$

in which  $u$ ,  $v$  and  $w$  are the velocity components in the Cartesian coordinates,  $V_m$  and  $p_m$  the velocity and pressure at the mitral section, and  $V_N$  the normal velocity on the ventricle wall. The first integral is the sum of the kinetic energy flux and the rate of work

done by pressure on the ventricular wall. The second integral is the time rate change of kinetic energy in the ventricle. The third integral is the total energy flux across the mitral annulus for blood flowing to the ventricle. The fourth term is the rate of work done by shear on the surface of the volume. The rate of work done by normal viscous stresses is very small and is omitted in Eq. (3). The last term is the rate of energy dissipation in the ventricle. Notice that all the energy terms are positive; the sign for each term of Eq. (3) is related to energy influx or out flux. Curve A in Fig. 8a is the kinetic energy flux delivered to blood from the ventricle during dilatation. It is presented in two scales in Fig. 8a and b for

comparison with other terms. Curve B is the total energy flux from LV dilatation to the flow. The gap between curves B and A indicates the rate of work done by pressure on the wall. Because the actual pressure is not known, the work done by pressure is based on a constant reference pressure (1333 Pa or 10 mmHg) at the apex. This simplification is to obtain the net rate of work done by pressure on the wall and that across the mitral annulus. The actual work done by pressure requires adding  $\Delta p_1(t)V_D(t)A_D(t)$  in which  $\Delta p_1(t)=p_A(t)-10\text{ mmHg}$ ,  $p_A(t)$ =the actual pressure at the apex, and  $A_D(t)$ =the cross sectional area of the mitral annulus. The gap between curves C and B is the rate change of kinetic energy in the ventricle. It is positive when curve C is higher than curve B, otherwise, negative. The distance between curves C and D is the rate of work done by pressure at the mitral annulus. The kinetic energy influx is indicated by the difference between curves D and E. It is about 5 times higher than that of kinetic energy flux from the ventricular wall (see curve A on Fig. 8a). The gap between curves E and F is the rate of work done by shear stresses on the wall. The rate of energy dissipation is presented by the difference between curves F and G. All the aforementioned curves are arranged so that the curve G represents the sum of the left hand side of Eq. (3); it should be zero. The small value shown by G indicates insignificant numerical residues; the work energy equation is well balanced. It also reflects that the velocity and pressure fields obtained from the Navier–Stokes equations are well checked by energy balance of Eq. (3).

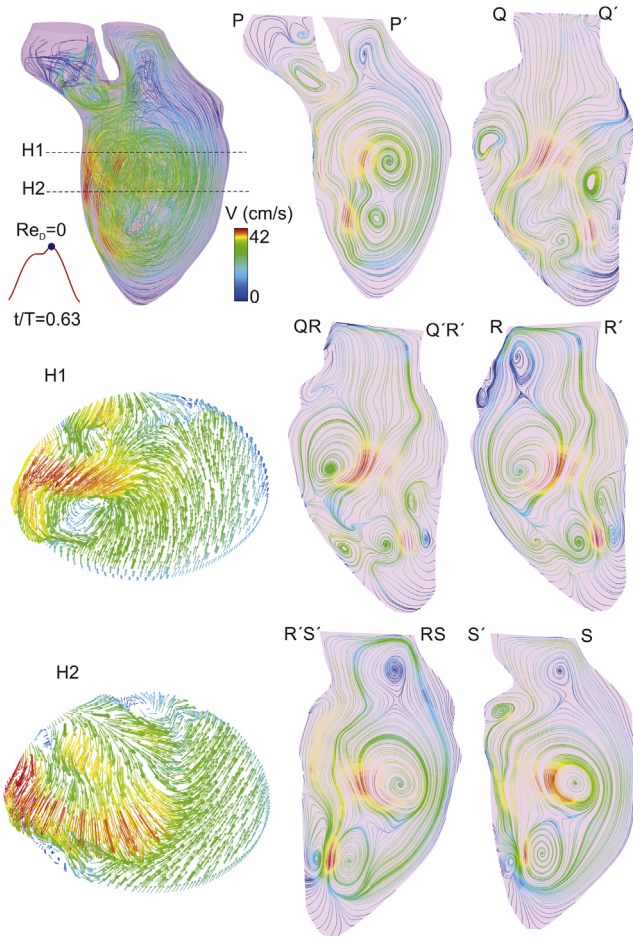


Fig. 6. Flow patterns and velocity vectors at the end of diastole;  $t/T=0.63$ .

#### 4. Conclusions

Based on MRI data of a normal ventricular contraction and dilatation, numerical solutions of the Navier–Stokes equations and the work-energy equation provide some insights into the kinematic, dynamic and energy characteristics of the mitral flow. At the onset of diastole, the outward momentum and suction produced by ventricular dilatation immediately disrupt vortices in the ventricle at end systole. The inflow is dominated by streamlines moving with the ventricle along with flow separation at the mitral orifice. The rapid growth of posterior and anterior crescent vortices forms an asymmetric ring vortex, providing a smooth transition for mitral flow to the ventricle. The diastolic deceleration results in rapid momentum transfer from the main flow to break up the ring vortex, forming a large counterclockwise core vortex. The inflow associated with the left atrial contraction is accompanied by changes in the vortices, balancing momentum in the ventricle. The work done by viscous stresses and dissipation energy are quantified to be small, and they are practically balanced

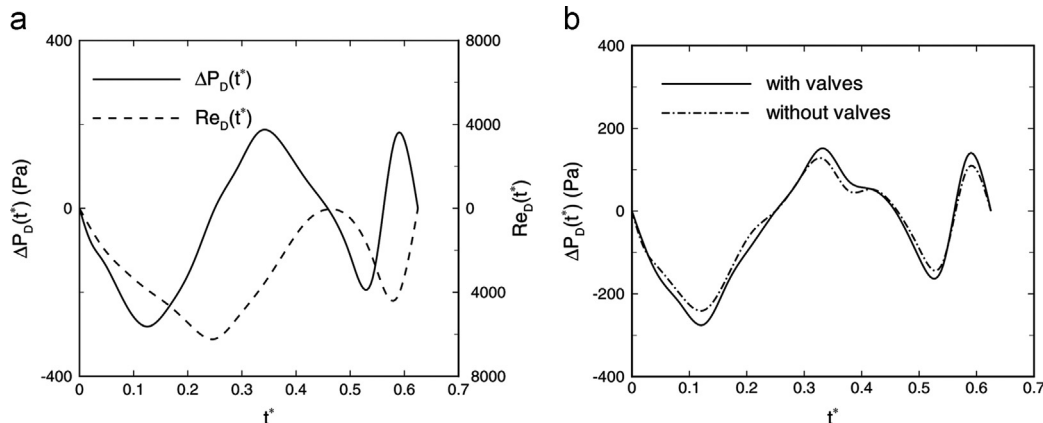
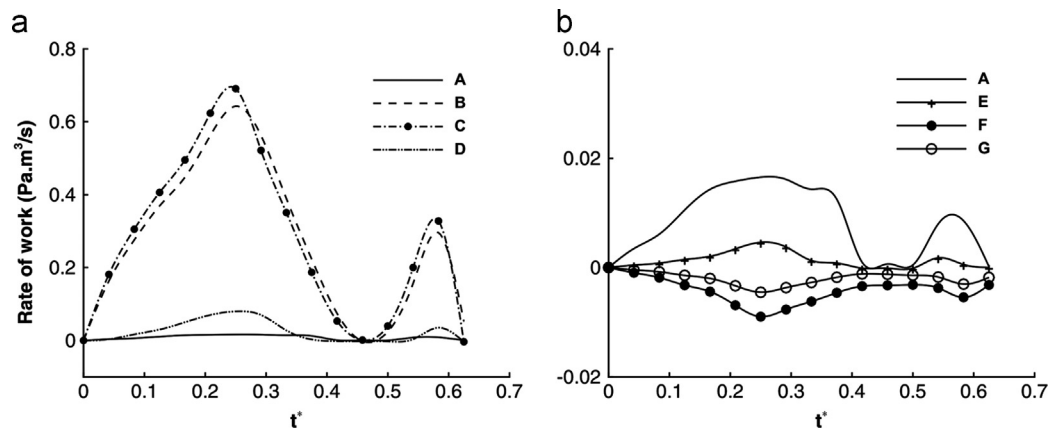


Fig. 7. (a) Time variation of Reynolds number with pressure drop during diastole and systole for 3D modelling of LV (b) Pressure drop for 2D modelling of LV with and without mitral valve leaflets.



**Fig. 8.** Rate of energy transfer of diastolic flow in the left ventricle: Curve A=kinetic energy flux on wall, (B–A)=rate work done by pressure on the wall, (C–B)=rate change of kinetic energy, (C–D)=rate of work by pressure at the outlet, (D–E)=kinetic energy influx, (E–F)=rate of work done by shear on the wall, and (G–F)=rate of energy dissipation.

with each other. Thus, the kinetic energy flux and the rate of work done by pressure on the ventricle are practically equal to the total energy influx at the mitral orifice and the rate change of kinetic energy in the ventricle. In other words, the total energy delivered from ventricular wall to blood is practically conserved in the ventricle during diastole.

## Acknowledgments

The study was supported by the University of Pittsburgh, the Nanyang Technological University, a Singapore International Graduate Award to S. S. Khalafvand, and a research grant to L. Zhong from the National Medical Research Council of Singapore Ministry of Health (NMRC/EDG/1037/2011).

## References

Baccani, B., Domenichini, F., Pedrizzetti, G., 2002. Vortex dynamics in a model left ventricle during filling. *Eur. J. Mech. B/Fluids* 21, 527–543.

Baccani, B., Domenichini, F., Pedrizzetti, G., 2003. Model and influence of mitral valve opening during the left ventricular filling. *J. Biomech.* 36, 355–361.

Bolger, A.F., Heiberg, E., Karlsson, M., Wigström, L., Engvall, J., Sigfridsson, A., Ebberts, T., Kvitting, J.-P.E., Carlhäll, C.J., Wranné, B., 2007. Transit of blood flow through the human left ventricle mapped by cardiovascular magnetic resonance. *J. Cardiovasc. Magn. Reson.* 9, 741–747.

Brown, T.D., Hung, T.-K., 1977. Computational and experimental investigations of two-dimensional nonlinear peristaltic flows. *J. Fluid Mech.* 83, 249–272.

Charonko, J., Kumar, R., Stewart, K., Little, W., Vlachos, P., 2013. Vortices formed on the mitral valve tips aid normal left ventricular filling. *Ann. Biomed. Eng.* 41, 1049–1061.

Cheng, Y., Oertel, H., Schenkel, T., 2005. Fluid-structure coupled CFD simulation of the left ventricular flow during filling phase. *Ann. Biomed. Eng.* 33, 567–576.

Domenichini, F., Pedrizzetti, G., Baccani, B., 2005. Three-dimensional filling flow into a model left ventricle. *J. Fluid Mech.* 539, 179–198.

Ebberts, T., Wigstrom, L., Bolger, A.F., Wranné, B., Karlsson, M., 2002. Noninvasive measurement of time-varying three-dimensional relative pressure fields within the human heart. *J. Biomech. Eng.* 124, 288–293.

Eriksson, J., Dyverfeldt, P., Engvall, J., Bolger, A.F., Ebberts, T., Carlhäll, C.J., 2011. Quantification of presystolic blood flow organization and energetics in the human left ventricle. *Am. J. Physiol. Heart Circ. Physiol.* 300, H2135–H2141.

Faludi, R., Szulik, M., D’Hooge, J., Herijgers, P., Rademakers, F., Pedrizzetti, G., Voigt, J.-U., 2010. Left ventricular flow patterns in healthy subjects and patients with prosthetic mitral valves: an in vivo study using echocardiographic particle image velocimetry. *J. Thorac. Cardiovasc. Surg.* 139, 1501–1510.

Hung, T.K., Balasubramanian, S.R., Simon, M.A., Suffoletto, M.S., Borovetz, H.S., Gorcsan, J., 2008. Hemodynamic information and analysis of cardiac pumping. *J. Mech. Med. Biol.* 8(1), 87–95.

Hung, T.-K., Tsai, T.M.-C., 1997. Kinematic and dynamic characteristics of pulsatile flows in stenotic vessels. *J. Eng. Mech.*, 123.

Hung, T.-K., Khalafvand, S.S., Ng, E.Y.-K., 2015. Fluid dynamic characteristics of systolic blood flow of the left ventricle. *J. Mech. Med. Biol.* 1550047.

Issa, R.I., 1986. Solution of the implicitly discretised fluid flow equation by operators-splitting. *J. Comput. Phys.* 62, 40–65.

Khalafvand, S.S., Zhong, L., Ng, E.Y.-K., 2014. Three-dimensional CFD/MRI modeling reveals that ventricular surgical restoration improves ventricular function by modifying intraventricular blood flow. *Int. J. Numer. Methods Biomed. Eng.* 30, 1044–1056.

Khalafvand, S.S., Hung, T.-K., Ng, E.Y.-K., Zhong, L., 2015. Kinematic, dynamic, and energy characteristics of diastolic flow in the left ventricle. *Comput. Math. Methods Med.* 2015, 12.

Kilner, P.J., Yang, G.-Z., Wilkes, A.J., Mohiaddin, R.H., Firmin, D.N., Yacoub, M.H., 2000. Asymmetric redirection of flow through the heart. *Nature* 404, 759–761.

Kim, W.Y., Walker, P.G., Pedersen, E.M., Poulsen, J.K., Oyre, S., Houliand, K., Yogannathan, A.P., 1995. Left ventricular blood flow patterns in normal subjects: a quantitative analysis by three-dimensional magnetic resonance velocity mapping. *J. Am. Coll. Cardiol.* 26, 224–238.

Krittian, S., Janoske, U., Oertel, H., Böhlke, T., 2010. Partitioned fluid–solid coupling for cardiovascular blood flow. *Ann. Biomed. Eng.* 38, 1426–1441.

Long, Q., Merrifield, R., Yang, G.Z., Xu, X.Y., Kilner, P.J., Firmin, D.N., 2003. The influence of inflow boundary conditions on intra left ventricle flow predictions. *J. Biomech. Eng.* 125, 922–927.

Long, Q., Merrifield, R., Xu, X.Y., Kilner, P., Firmin, D.N., Yang, G.Z., 2008. Subject-specific computational simulation of left ventricular flow based on magnetic resonance imaging. *Proc. Inst. Mech. Eng. Part H: J. Eng. Med.* 222, 475–485.

Macagno, E.O., Hung, T.-K., 1967. Computational and experimental study of a captive annular eddy. *J. Fluid Mech.* 28, 43–64.

McQueen, D.M., Peskin, C.S., 1989. A three-dimensional computational method for blood flow in the heart. II. contractile fibers. *J. Comput. Phys.* 82, 289–297.

McQueen, D.M., Peskin, C.S., 1997. Shared-memory parallel vector implementation of the immersed boundary method for the computation of blood flow in the beating mammalian heart. *J. Supercomput.* 11, 213–236.

McQueen, D.M., Peskin, C.S., 2000. A three-dimensional computer model of the human heart for studying cardiac fluid dynamics. *Comput. Graph* 34, 56–60.

Pedrizzetti, G., Domenichini, F., 2005. Nature optimizes the swirling flow in the human left ventricle. *Phys. Rev. Lett.* 95, 108101.

Roache, P.J., 1998. Verification and Validation in Computational Science and Engineering. Hermosa Publishers, Albuquerque, New Mexico.

Saber, N., Gosman, A.D., Wood, N., Kilner, P., Charrier, C., Firmin, D., 2001. Computational flow modeling of the left ventricle based on in vivo MRI data: initial experience. *Ann. Biomed. Eng.* 29, 275–283.

Saber, N.R., Wood, N.B., Gosman, A.D., Merrifield, R.D., Yang, G.-Z., Charrier, C.L., Gatehouse, P.D., Firmin, D.N., 2003. Progress towards patient-specific computational flow modeling of the left heart via combination of magnetic resonance imaging with computational fluid dynamics. *Ann. Biomed. Eng.* 31, 42–52.

Schenkel, T., Malve, M., Reik, M., Markl, M., Jung, B., Oertel, H., 2009. MRI-based CFD analysis of flow in a human left ventricle: methodology and application to a healthy heart. *Ann. Biomed. Eng.* 37, 503–515.

Uejima, T., Koike, A., Sawada, H., Aizawa, T., Ohtsuki, S., Tanaka, M., Furukawa, T., Fraser, A.G., 2010. A new echocardiographic method for identifying vortex flow in the left ventricle: numerical validation. *Ultrasound Med. Amp. Biol.* 36, 772–788.

Vierendeels, J.A., Riemslag, K., Dick, E., Verdonck, P.R., 2000. Computer simulation of intraventricular flow and pressure gradients during diastole. *J. Biomech. Eng.* 122, 667–674.

Watanabe, H., Sugiura, S., Kafuku, H., Hisada, T., 2004. Multiphysics simulation of left ventricular filling dynamics using fluid–structure interaction finite element method. *Biophys. J.* 87, 2074–2085.